

## Meso-scale based parameter identification for 3D concrete plasticity model

Samir Suljevic<sup>\*1,3</sup>, Adnan Ibrahimbegovic<sup>1,2a</sup>, Emir Karavelic<sup>3b</sup> and Samir Dolarevic<sup>3c</sup>

<sup>1</sup>Université de Technologie de Compiègne, Laboratoire Roberval de Mécanique,  
Centre de Recherche Royallieu, 60200 Compiègne, France

<sup>2</sup>Institut Universitaire de France, France

<sup>3</sup>Faculty of Civil Engineering, University of Sarajevo, Patriotske lige 30, Sarajevo 71000,  
Bosnia and Herzegovina

(Received December 9, 2021, Revised December 17, 2021, Accepted December 29, 2021)

**Abstract.** The main aim of this paper is the identification of the model parameters for the constitutive model of concrete and concrete-like materials capable of representing full set of 3D failure mechanisms under various stress states. Identification procedure is performed taking into account multi-scale character of concrete as a structural material. In that sense, macro-scale model is used as a model on which the identification procedure is based, while multi-scale model which assume strong coupling between coarse and fine scale is used for numerical simulation of experimental results. Since concrete possess a few clearly distinguished phases in process of deformation until failure, macro-scale model contains practically all important ingredients to include both bulk dissipation and surface dissipation. On the other side, multi-scale model consisted of an assembly micro-scale elements perfectly fitted into macro-scale elements domain describes localized failure through the implementation of embedded strong discontinuity. This corresponds to surface dissipation in macro-scale model which is described by practically the same approach. Identification procedure is divided into three completely separate stages to utilize the fact that all material parameters of macro-scale model have clear physical interpretation. In this way, computational cost is significantly reduced as solving three simpler identification steps in a batch form is much more efficient than the dealing with the full-scale problem. Since complexity of identification procedure primarily depends on the choice of either experimental or numerical setup, several numerical examples capable of representing both homogeneous and heterogeneous stress state are performed to illustrate performance of the proposed methodology.

**Keywords:** concrete failure model; embedded discontinuity; multi-surface yield criteria; multiscale approach; optimization; parameter identification; strong coupling

---

### 1. Introduction

In the last few decades, heterogeneous materials have been widely used in various fields of industry such as civil, mechanical, aerospace engineering, etc. and there is tendency for their

---

\*Corresponding author, Ph.D. Student, E-mail: samir.suljevic@utc.fr, samir.suljevic@gf.unsa.ba

<sup>a</sup>Professor, E-mail: adnan.ibrahimbegovic@utc.fr

<sup>b</sup>Assistant Professor, E-mail: emir.karavelic@gf.unsa.ba

<sup>c</sup>Professor, E-mail: samir.dolarevic@gf.unsa.ba

increasing application. First of all, this development is initiated by contemporary achievements in material technology that enable a rapid trend of producing of high performance materials. In addition, an implementation of numerical methods in terms of use with modern computers, with optimized calculation algorithms have enabled obtaining results pretty quickly on quite complex models with satisfactory accuracy. Hence, the representation of discretized fields of interest such as displacement field, stress field, etc. can be obtained in a rather straightforward way.

In this paper, the focus is put on the parameter identification of the plasticity constitutive model capable of describing the failure of massive structures built by concrete and concrete-like materials. The identification procedure is performed in the spirit of the multiscale approach, while previously stated plasticity constitutive model acting as a macro-scale model is used as a model on which identification procedure is based and pure multiscale model with strong coupling between fine and coarse scale is used for a numerical simulation of experimental results. Due to specific model structure featured by well-defined and clear physical interpretation of its parameters, we are allowed to divide identification procedure in three completely separate stages. Furthermore, influence of each of these parameters is limited only to clearly defined phase of material behavior (elastic, hardening or softening) leading to substantial reduction in computational time and resulting in great simplification of the identification procedure itself.

In the context of model structure for identification procedure, 3D macro-scale model capable of representing a full set of 3D failure modes in tension, compression and shear is utilized for numerical reproduction of a very complex nature of the material with a pronounced heterogeneity of internal structure that directly affects the behavior under the action of different quasi-static load cases. This model of concrete-like materials considers multi-surface plasticity with Drucker-Prager yield criteria governing hardening behavior and strain softening behavior is represented with St-Venant criterion in strain space defined by three surface as explained in the Section 2. In the spirit of multiscale approach, this macro-scale model can represent initial stages of concrete cracking followed by a large number of narrow cracks in a concrete domain close to surface, their coalescence inside the element and gradual propagation until fully developed failure mode with clearly visible macro-cracks triggered with St-Venant plasticity criterion in strain space, as previously stated.

On the other side, multiscale model with embedded discontinuity discrete approximation is utilized for numerical simulations of various kinds of experimental results. In this way structural failure modeling can be very successfully performed by assuming homogenized response on macro-scale, incorporating damage mechanisms and 3D failure modes defined at micro-scale. Each macro-scale element represents the domain of micro-scale elements in such a way that the set of micro-scale elements completely fits inside the macro-element domain. For the purpose of establishing compatibility between both scales assuming strong scale coupling, constraint over displacement field is imposed over the macro-element boundary producing highly efficient displacement based coupling in the spirit of localized Lagrange multipliers.

An efficient framework for dealing with localized failure is enabled through implementation of embedded discontinuity inside the macro-scale elements. A proposed methodology can provide a full insight into reproducing of 3D failure modes with very satisfying performance regardless of the stress state in the element. A more detailed description of model setup is presented in the Section 3.

The sequential identification approach employed in this work is accomplished due the fact that all macro-scale parameters have a clear physical interpretation and its limit only to a clearly defined phase of material behavior (elastic, hardening or softening). The two most significant advantages of this approach are: first, simplification through solving individual identification steps individually instead of solving full-scale problems and, as a second, only part of a test simulation for each of the

three stages can be performed leading to substantial computational time savings.

Optimization algorithm used to find minimum of objective function adopted in this work is downhill simplex or Nelder-Mead method. The Nelder-Mead method attempts to minimize a scalar-valued nonlinear function of  $n$  real variables using only function values, without any derivative information (explicit or implicit) (Lagarias *et al.* 1998). It is worth mentioning that variety of techniques is available for procedure of identification parameters via optimization methods (Mahnken 2004, Kucerova *et al.* 2009) such as gradient-based methods, stochastic evolutionary algorithms and adaptive smoothing of objective function by artificial neural networks.

Gradient-based methods have been widely used in various identification problems due to its computationally efficient optimization algorithms. Iacono *et al.* (2006) provide a parameter identification for gradient-enhanced continuum damage model analyzing tensile behavior of concrete as an important feature to have a clearer insight in the mechanisms governing the fracture process. Mahnken and Stein (1995) presents a strategy for identification of material parameters of viscoplastic constitutive equation from uniaxial test. Least squares functional are minimized by gradient based descent method, while stability of numerical results for material results is investigated by use of the eigenvalues for the Hessian of the least squares-functional. Mahnken (2004) deals with parameter identification for constitutive equations on the basis of experimental data by introducing four different identification methods for analyzing inverse problems illustrated by simple examples. Meier *et al.* (2005) presents inverse analysis in fracture mechanics which, among other areas of application, can also be used for deterministic characterization of concrete-like materials by traditional three-point-bending tests. In a case when sensitivity determination is fairly difficult, the accuracy between numerical and “exact” sensitivities is driven by the choice of the pseudo-time step used in numerical simulation. In order to reduce computational time, pseudo-time should be as large as possible leading to non-smooth response based objective function. As a result, the gradient-based methods are unlikely to be very successful (Kucerova *et al.* 2009).

Alternatively, stochastic evolutionary algorithm as a soft-computing technique have been used in many recent works for obtaining solution of identification procedure on a level of either material (Ibrahimbegovic *et al.* 2021) or on a level of simple structures (Furukawa and Yagawa 1997, Ibrahimbegovic *et al.* 2004, Lepš 2005, Pyrz and Zairi 2007). In addition to previous approaches, adaptive smoothing of objective function by an artificial neural network can be used as a technique for identification procedure. Kucerova *et al.* (2009) describes parameter identification of damage model whose approximation is provided by the radial basis function network (RBFN). Waszczyszyn and Ziemiański (2006) show the application of this approach in the analysis of various problems such as the identification of damage parameters of steel beam, concrete fatigue durability and soil-structure interaction, while Pichler *et al.* (2003) proposes a parameter identification method for determination of unknown model parameters in geotechnical engineering. Similar goal is followed in Kozar *et al.* (2018) for fiber reinforced concrete.

The main novelty of this work is the procedure of parameter identification that can be carried out either on a basis of standard experimental results or numerical simulation results. We compare and advise on these two alternatives for identification and give some recommendations for preserving robustness of the proposed procedure. In this work, the procedure of parameter identification in each phase is implemented, by using the software MATLAB and FEAP. While FEAP is used for finite element analysis (FEA) for the corresponding material parameters, MATLAB is used for obtaining objective functions and its minimization assuming the Nelder-Mead algorithm. In the fourth section of the paper, objective functions for particular stages of material behavior are presented.

The outline of the paper is as follows. In the next section, description of a macro-scale multi

surface plasticity yield criteria is presented. Description of the multiscale model with embedded discontinuity discrete approximation is presented in third section. The complete description of macro-scale model is presented in Karavelic *et al.* (2019), while the multiscale model is presented in details in Ibrahimbegovic *et al.* (2021). In fourth section a review of used either numerical or experimental setup is presented, while results of parameter identification procedure with remarks on the optimization procedure for each stage of material behavior is described in fifth section. The last section provides the conclusions with some remarks on perspectives.

## 2. Macro-scale model description

In the following section we present macro-scale model on which identification procedure is based. In that context, multi-surface plasticity model of concrete that can reproduce full set of 3D failure modes for tension, compression and shear is considered. From pure mechanical and empirical view, it is known that concrete passes through several clearly distinguish phases in a process of deformation starting by creation of the fracture process zone with larger number of micro-cracks and subsequent fully developed failure mode with macro-crack clearly visible in final crack pattern.

These effects are recognized in the model in such a way that the fracture process zone is represented with non-associated Drucker-Prager plasticity criterion with hardening, while macro-crack is represented with strong displacement discontinuity in the spirit of embedded discontinuity FEM.

In order to describe macro-scale model in following we define three main ingredients for constitutive model of plasticity sufficient for the stress tensor computation as well as internal variables evolution:

- additive decomposition of total strain into elastic and plastic component by assuming the independence of the elastic response on plastic flow

$$\boldsymbol{\varepsilon} = \boldsymbol{\varepsilon}^e + \boldsymbol{\varepsilon}^p \quad (1)$$

- the free energy function constructed as a quadratic form in terms of deformation assuming that elastic response remains linear and thus reducing to Hooke's law

$$\psi(\boldsymbol{\varepsilon}, \boldsymbol{\varepsilon}^p, \zeta) = \frac{1}{2}(\boldsymbol{\varepsilon} - \boldsymbol{\varepsilon}^p) \cdot \hat{\mathbf{C}}(\boldsymbol{\varepsilon} - \boldsymbol{\varepsilon}^p) + \frac{1}{2}\zeta K \zeta \quad (2)$$

- the yield criterion shown in Fig. 1 which corresponds to the classical Drucker-Prager model as a function of stress tensor  $\boldsymbol{\sigma}$  and stress-like internal variable  $q$

$$\phi_y(\boldsymbol{\sigma}, q) = \|\text{dev}[\boldsymbol{\sigma}]\| + \frac{1}{3}\tan(\varphi)\text{tr}[\boldsymbol{\sigma}] - \sqrt{\frac{2}{3}}(\sigma_y - q) \quad (3)$$

while plastic potential function is slightly different from yield function and defined as

$$\phi_{p,s}(\boldsymbol{\sigma}, q) = \|\text{dev}[\boldsymbol{\sigma}]\| + \frac{1}{3}\tan(\varphi)\text{tr}[\boldsymbol{\sigma}] \quad (4)$$

where  $\|\text{dev}[\boldsymbol{\sigma}]\|$  is the deviatoric part of the stress tensor,  $\|\boldsymbol{\sigma}\| = \sqrt{\boldsymbol{\sigma}:\boldsymbol{\sigma}}$  is the Frobenius norm,  $\tan(\varphi)$  is material parameter that can characterize the internal friction,  $\tan(\psi)$  is material parameter describing the angle of dilatancy and  $\sigma_y$  is uniaxial yield stress identified from a tension

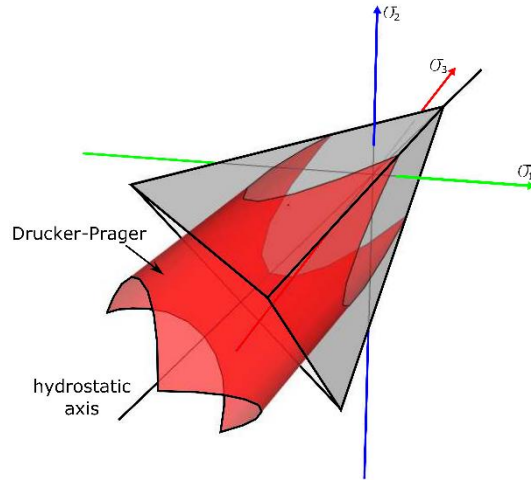


Fig. 1 Multisurface plasticity criterion in plasticity stress space (Karavelic *et al.* 2019)

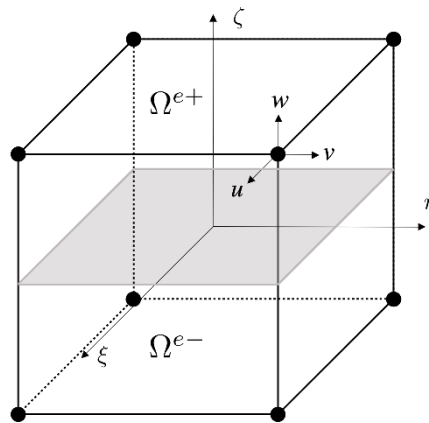


Fig. 2 Displacement discontinuity surface in localized element dividing domain into  $\Omega^{e+}$  and  $\Omega^{e-}$  (Ibrahimbegovic *et al.* 2021)

test.

It should be emphasized that the material instability occurs even in hardening phase in latter case of difference between plastic potential and yield function as one of practical consequences of the presented model setup. Furthermore, another material instability referred to typical case is associated with the softening. Standard finite element implementation is enriched by strong discontinuity formulation, which is adopted for representing the cracking of concrete both in tension and compression, in a very similar manner as for the incompatible mode method.

In particular, in tension we can observe elastic stage accompanied by unstable softening branch, while in compression we can observe three different deformation stage: linear elastic, nonlinear inelastic and localized softening as in standard stress-strain diagram of concrete. Naturally, behavior representing of massive structures with macro-scale model is achieved by including the following dissipative mechanisms:

1. bulk dissipation characterized by the initiation and development of micro-cracks (contribution

of fracture process zone)

2. surface dissipation at the level of the localization zones represented by a discontinuity surface in terms of macro-cracks triggered by St-Venant plasticity criterion

The latter is defined in strain space defined by three surfaces, but it can be written in standard format in stress space

$$\begin{aligned}\phi_1(\boldsymbol{\sigma}) &= \frac{3K+G}{9KG}\sigma_1 - \frac{3K-2G}{18KG}(\sigma_2 + \sigma_3) - (\sigma_y - q) \leq 0 \\ \phi_2(\boldsymbol{\sigma}) &= \frac{3K+G}{9KG}\sigma_2 - \frac{3K-2G}{18KG}(\sigma_1 + \sigma_3) - (\sigma_y - q) \leq 0 \\ \phi_3(\boldsymbol{\sigma}) &= \frac{3K+G}{9KG}\sigma_3 - \frac{3K-2G}{18KG}(\sigma_1 + \sigma_2) - (\sigma_y - q) \leq 0\end{aligned}\quad (5)$$

In the proposed model, the softening constitutive law is chosen in exponential form implying the following expression for stress-like internal variable for plasticity

$$\bar{q} = \sigma_y \left( 1 - \exp\left(-\bar{\zeta} \frac{\sigma_y}{G_f}\right) \right) \quad (6)$$

where  $G_f$  is the fracture energy parameter for which the appropriate value should be chosen to provide appropriate representing of the inelastic micro-cracking mechanisms in compression and tension (Ibrahimbegovic 2009).

As illustrated in Fig. 3, corresponding amount of fracture energy can be substantially different for tension and compression failure mechanisms due to typically large discrepancy in number of cracks.

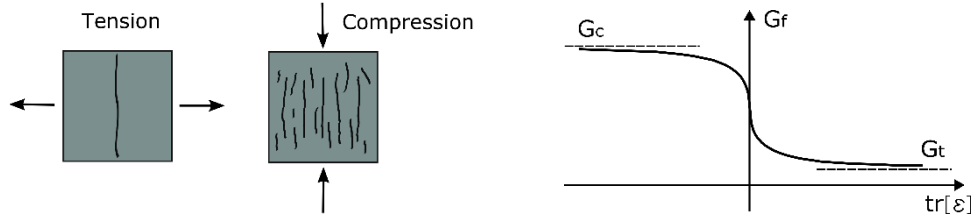


Fig. 3 Crack patterns for tension and compression failure mechanisms with corresponding fracture energies (Karavelic *et al.* 2019)

Spatial discretization of domain is performed by using 3D 8-node hexahedron element providing standard discretization procedure to construct the finite element based displacement approximation. On the other side, time discrete approximation is carried out numerically by using the unconditionally stable backward Euler time integration scheme in the spirit of the operator split method.

The weak form of equilibrium can be written as a system of global and local equilibrium equations.

$$A_{e=1}^{n_{el}} (\mathbf{f}^{int,(e)} - \mathbf{f}^{ext}) = 0; \quad \mathbf{f}^{int,(e)} = \int_{\Omega^e} \mathbf{B}^T \cdot \boldsymbol{\sigma}_{n+1} dV$$

$$\mathbf{h}_{n+1}^{(e)} = \int_{\Omega^e} \overline{\mathbf{G}}_v^T(\mathbf{x}) \cdot \boldsymbol{\sigma}_{n+1} dV + \int_{\Gamma_s} t_{m,n+1} dA; \quad \forall e \in [1, n_{el}] \quad (7)$$

The final set of equilibrium equations after performing consistent linearization can be written for a time step  $t_{n+1}$  and iteration ( $i$ )

$$\begin{aligned} A_{e=1}^{n_{el}} \left[ \mathbf{K}_{n+1}^{e,(i)} \Delta \mathbf{u}_{n+1}^{(i)} + \mathbf{F}_{n+1}^{e,(i)} \Delta \boldsymbol{\alpha}_{n+1}^{(i)} \right] &= A_{e=1}^{n_{el}} \left[ \mathbf{f}_{n+1}^{ext,e} - \mathbf{f}_{n+1}^{int,e,(i)} \right] \\ \mathbf{h}_{n+1}^{e,(i)} + \left( \mathbf{F}_{v,n+1}^{e,(i)} + \mathbf{K}_{d,n+1}^{(i)} \right) \Delta \mathbf{u}_{n+1}^{(i)} + \left( \mathbf{H}_{n+1}^{e,(i)} + \mathbf{K}_{\alpha,n+1}^{(i)} \right) \Delta \boldsymbol{\alpha}_{n+1}^{(i)} &= 0 \end{aligned} \quad (8)$$

where

$$\begin{aligned} \mathbf{K}_{n+1}^{e,(i)} &= \int_{\Omega^e} \mathbf{B}^T \mathbf{C}_{n+1}^{ep,(i)} \mathbf{B} dV, \quad \mathbf{F}_{n+1}^{e,(i)} = \int_{\Omega^e} \mathbf{B}^T \mathbf{C}_{n+1}^{ep,(i)} \overline{\mathbf{G}}_m dV \\ \mathbf{F}_{v,n+1}^{e,(i)} &= \int_{\Omega^e} \mathbf{m}^T \overline{\mathbf{G}}^T \mathbf{C}_{n+1}^{ep,(i)} \mathbf{B} dV \\ \mathbf{H}_{n+1}^{e,(i)} &= \int_{\Omega^e} \mathbf{m}^T \overline{\mathbf{G}}^T \mathbf{C}_{n+1}^{ep,(i)} \overline{\mathbf{G}}_m^T dV \\ \mathbf{K}_{d,n+1}^{e,(i)} &= A_{\Gamma_s^e} \frac{\partial t_m}{\partial u} \Big|_{n+1}^{(i)}, \quad \mathbf{K}_{\alpha,n+1}^{e,(i)} = A_{\Gamma_s^e} \frac{\partial t_m}{\partial \alpha} \Big|_{n+1}^{(i)} \end{aligned}$$

In this way, displacement jump increment  $\Delta \boldsymbol{\alpha}_{n+1}^{(i)}$  can be obtain for a given value of the displacement field increment  $\Delta \mathbf{u}_{n+1}^{(i)}$  by solving second equation of previously stated set taking advantage that is written locally in each localized element.

### 3. Multiscale model description

In this section, multiscale model with enriched discrete approximation by introducing embedded discontinuity inside the localized element is presented. In the context of parameter identification procedure, the model is utilized for numerical simulation of various kinds of experimental results.

In the spirit of a multiscale approach, macro-scale is used for description of homogeneous structural response, while micro-scale is utilized for representing full set of 3D inelastic damage mechanisms. Both 4-node tetrahedron and 8-node hexahedron are implemented for spatial macro-scale discretization, while micro-scale mesh consists of an assembly of Timoshenko beam in a lattice form featuring the plasticity model is able to represent localized failure in mode I, mode II and mode III.

The proposed model is based on strong coupling between coarse and fine scale using displacement based coupling. It implies continually exchanging information between scales during the numerical analysis and the computation advances simultaneously on both scales. Since nonlinearity effects occur practically from the start of analysis, both macro and micro-scale iterative computations are executed with one iterative sweep at macro-scale accompanied by many iterations at micro-scale at each time step. From practical point of view in terms of FEM, this should provide admissible solution for current iterative values at macro-scale. Let us mention that solely when convergence is achieved at both scales, the computation progress to the next time. The computation is carried out in the spirit of the operator split method.

Considering the essential settings of finite element method (FEM), the constitutive equations commonly are not defined on the macro-element implying its element arrays are obtained from the

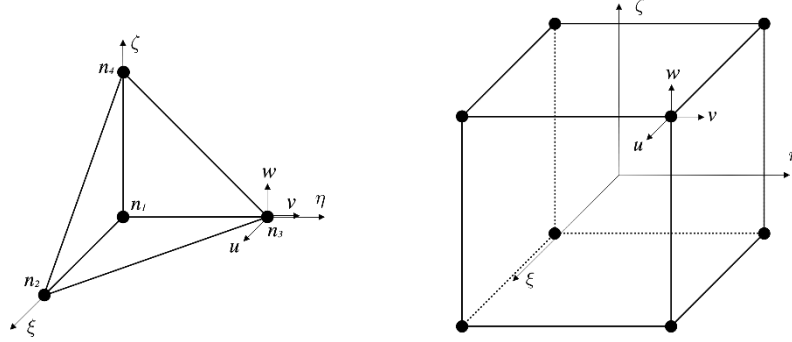


Fig. 4 3D isoparametric macro-scale element: 4-node tetrahedron and 8-node hexahedron (Ibrahimbegovic *et al.* 2021)

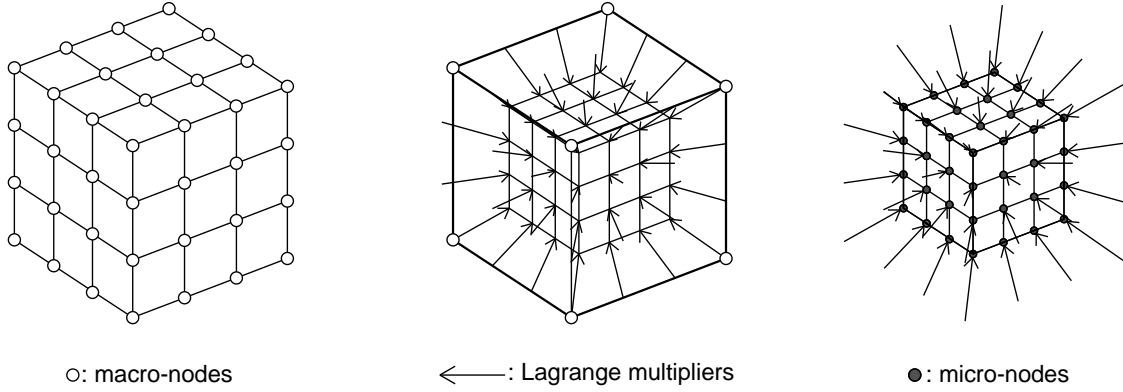


Fig. 5 Macro and micro-scale element mesh connected in the spirit of Lagrange multipliers over a macro-element boundary (Ibrahimbegovic *et al.* 2021)

corresponding micro-scale computations. Besides the particular individual settings of micro and macro-scale, it is essential to provide the compatibility between them. In that context, localized Lagrange multiplier method is utilized which allows setting a constraint on the discrete displacement field over the boundary of macro-elements. Consequently, computation of macro-element tangent stiffness matrix as well as residual vectors is performed by an assembly of micro-scale elements contributions, which are statically condensed at the macro scale.

The representation of the localized failure on the macro-scale level is performed within a framework of the incompatible mode method presented in (Ibrahimbegovic and Wilson 1991). The incompatible mode function  $M$  for a macro-scale element in the natural coordinate space  $(\xi, \eta, \zeta)$  can be written as

$$M(\xi, \eta, \zeta) = H_{\Gamma_s}(\xi, \eta, \zeta) - \sum_{b \in \Omega^{e+}} N_b^M(\xi, \eta, \zeta) \quad (9)$$

where  $H_{\Gamma_s}(\xi, \eta, \zeta)$  is the Heaviside step function.

For a localized macro-element crossed by discontinuity, macro-scale element displacement field accounting for the incompatible mode function  $M$  and displacement jump  $\alpha^{M,E}$  can be written as

$$\mathbf{u}_{n+1}^M|_{\Gamma^{Mm,E}}(\mathbf{x}^m) = \sum_{a \in \Gamma^{Mm,E}} \mathbf{N}_a^{M,E}(\mathbf{x}^m) \mathbf{d}_{a,n+1}^{M,E} + \mathbf{M}^{M,E} \boldsymbol{\alpha}_{n+1}^{M,E} \quad (10)$$

where  $\mathbf{N}_a^{M,E}$  are macro-scale shape functions and  $\mathbf{d}_{a,n+1}^{M,E}$  is macro-scale displacement field.

As previously stated, micro-scale nodal displacements can be written accounting for crack opening and Lagrange multiplier method as

$$\bar{\mathbf{d}}_{n+1}^m|_{\Gamma^{M,E}} = \mathbf{T}^E \mathbf{d}_{n+1}^{M,E} + \mathbf{S}^E \boldsymbol{\alpha}_{n+1}^{M,E} \quad (11)$$

where  $\mathbf{T}$  and  $\mathbf{S}$  are element connectivity matrices based on particular values of macro-scale shape functions and incompatible mode function, respectively.

By solving linearized system of the equations at macro-scale

$$\begin{bmatrix} \mathbf{K}^M & \mathbf{F}^M \\ \mathbf{F}^{M,T} & \mathbf{H}^M \end{bmatrix} \begin{bmatrix} \Delta \mathbf{d}^M \\ \Delta \boldsymbol{\alpha}^M \end{bmatrix} = - \begin{bmatrix} \mathbf{r}^M \\ \mathbf{h}^M \end{bmatrix} \quad (12)$$

we can compute firstly displacement jump increment on macro-scale, and then the increment of displacement field on macro-scale. In previous equation, sub-matrices can be computed in a manner of constraint Eq. (12)

$$\begin{aligned} \mathbf{K}_{n+1}^{M,E} &= \mathbf{T}^{E,T} \tilde{\mathbf{K}}_{n+1}^m \mathbf{T}^E \\ & \begin{matrix} (N \times N) & (N \times n_\Gamma) & (n_\Gamma \times n_\Gamma) & (n_\Gamma \times N) \end{matrix} \\ \mathbf{F}_{n+1}^{M,E} &= \mathbf{T}^{E,T} \tilde{\mathbf{K}}_{n+1}^m \mathbf{S}^E \\ & \begin{matrix} (N \times 3) & (N \times n_\Gamma) & (n_\Gamma \times n_\Gamma) & (n_\Gamma \times 3) \end{matrix} \\ \mathbf{H}_{n+1}^{M,E} &= \mathbf{S}^{E,T} \tilde{\mathbf{K}}_{n+1}^m \mathbf{S}^E \\ & \begin{matrix} (3 \times 3) & (3 \times n_\Gamma) & (n_\Gamma \times n_\Gamma) & (n_\Gamma \times 3) \end{matrix} \end{aligned} \quad (13)$$

On the other side, Timoshenko beam finite elements in a lattice form are used for constructing micro-scale discrete approximation (Hadzalic *et al.* 2019, Karavelic *et al.* 2019). 3D micro-scale mesh is constructed by domain division into Voronoi cells while adjacent cells are connected by cohesive links. In this way, the displacement jump in the middle of the beam element can be very successfully simulated assuming the crack initiates and propagates at the interface of an adjacent Voronoi cells. The adopted beam plasticity model is capable of representing failure mechanisms in crack opening mode (mode I), as well as in in-plane and out-of plane sliding (mode II and mode III).

The finite element interpolation of the total micro displacement field within the incompatible mode framework can be written as

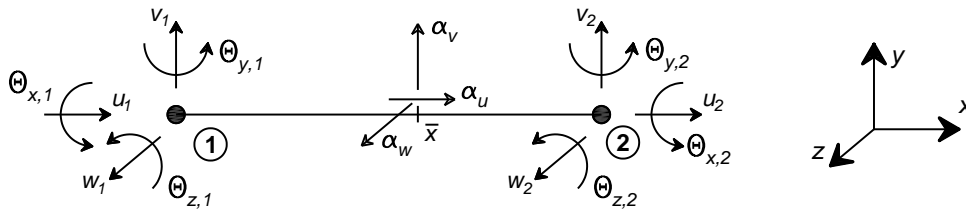


Fig. 6 Geometry and degrees of freedom for Timoshenko beam finite element (Ibrahimbegovic *et al.* 2021)

$$\mathbf{u}^m(x) = \sum_{a=1}^2 N_a(x) \mathbf{d}_a^m + M(x) \boldsymbol{\alpha}^m \quad (14)$$

where  $\mathbf{d}_a^m$  is micro-scale displacement vector and  $\boldsymbol{\alpha}^m$  is the micro-scale displacement jump vector.

Similarly, enhanced strain field can be written as

$$\boldsymbol{\varepsilon} = \sum_{a=1}^2 \mathbf{B}_a \mathbf{d}_a + \mathbf{G} \boldsymbol{\alpha} \quad (15)$$

where the matrix  $\mathbf{B}_a$  contains the derivatives of the shape functions and the matrix  $\mathbf{G}$  contains the derivatives of the incompatible mode function  $G(x)$  that can be split into regular  $\bar{G}(x)$  and singular part  $\bar{\bar{G}}(x)$ .

$$G(x) = \bar{G}(x) + \bar{\bar{G}}(x), \quad \bar{G}(x) = -\frac{1}{L^e}, \quad \bar{\bar{G}}(x) = \delta_{\bar{x}}(x)$$

In micro-scale framework, the weak form of equilibrium can be written as a system of global and local equilibrium equations

$$\begin{aligned} \mathbf{A}[\mathbf{f}_{int}^{m,e} - \mathbf{f}_{ext}^{m,e}] &= 0 \\ \mathbf{h}^{m,e} &= 0 \end{aligned} \quad (16)$$

The final set of equilibrium equations after performing consistent linearization can be written for a time step  $t_{n+1}$

$$\begin{bmatrix} \mathbf{K}^m & \mathbf{F}^m \\ \mathbf{F}_v^m + \mathbf{K}_d^m & \mathbf{H}^m + \mathbf{K}_a^m \end{bmatrix} \begin{bmatrix} \Delta \mathbf{d}_{n+1}^m \\ \Delta \boldsymbol{\alpha}_{n+1}^m \end{bmatrix} = - \begin{bmatrix} \mathbf{f}_{int,n+1}^m - \mathbf{f}_{ext,n+1}^m \\ \mathbf{h}^m \end{bmatrix} \quad (17)$$

where tangent stiffness matrices are defined in the following form:

$$\begin{aligned} \mathbf{K}_{n+1}^{m,e,(i)} &= \int_0^{L^e} \mathbf{B}^{e,T} \mathbf{C}_{n+1}^{(i)} \mathbf{B}^e dx \\ \mathbf{F}_{n+1}^{m,e,(i)} &= \int_0^{L^e} \mathbf{B}^{e,T} \mathbf{C}_{n+1}^{(i)} \bar{\mathbf{G}}^e dx \\ \mathbf{F}_{v,n+1}^{m,e,(i)} &= \int_0^{L^e} \bar{\mathbf{G}}^{e,T} \mathbf{C}_{n+1}^{(i)} \mathbf{B}^e dx \\ \mathbf{H}_{n+1}^{m,e,(i)} &= \int_0^{L^e} \bar{\mathbf{G}}^{e,T} \mathbf{C}_{n+1}^{(i)} \bar{\mathbf{G}}^e dx \end{aligned}$$

The increment of displacement jump vector  $\Delta \boldsymbol{\alpha}_{n+1}^m$  can be computed after performing static condensation in the following form

$$\Delta \boldsymbol{\alpha}_{n+1}^m = -(\mathbf{H}^m + \mathbf{K}_a^m)^{-1} (\mathbf{F}_v^m + \mathbf{K}_d^m) \Delta \mathbf{d}_{n+1}^m \quad (18)$$

By substituting  $\Delta \boldsymbol{\alpha}_{n+1}^m$  back into eq. 1, the increment of the displacement vector  $\Delta \mathbf{d}_{n+1}^m$  can be written as

$$[\mathbf{K}^m - \mathbf{F}^m (\mathbf{H}^m + \mathbf{K}_a^m)^{-1} (\mathbf{F}_v^m + \mathbf{K}_d^m)] \Delta \mathbf{d}_{n+1}^m = -(\mathbf{f}_{int,n+1}^m - \mathbf{f}_{ext,n+1}^m) \quad (19)$$

#### 4. Parameter identification procedure

The proposed identification procedure relies on experimental measurements (typically displacements and total force on testing machine) and on numerical results obtained by multiscale model simulations (energy, dissipation). We make an effort to be able to use experimental results and optimize this identification procedure without limitation only to experimental measurements.

Particularly, there are eleven independent material properties to be identified:

- a) Elastic parameters: Bulk modulus  $K$  and shear modulus  $G$
- b) Hardening parameters: uniaxial yield stress  $\sigma_y$ , angle of internal friction  $\tan(\varphi)$ , angle of dilatancy  $\tan(\psi)$ , hardening modulus for linear hardening  $K_{h,lin}$  and hardening parameter  $\beta$  that governs the rate with which saturation is achieved
- c) Softening parameters: Limit stress until stress increase  $\sigma_\infty$ , ultimate stress which triggers the softening  $\sigma_u$ , fracture energy in tension  $G_{f,t}$  and fracture energy in compression  $G_{f,c}$

In a broad sense, identification procedure analysis is carried in two essential step:

1. The definition of objective function based on experimental results or, in case of data deficiency, based on numerical simulations capable of representing all fields of interest in successfully way.
2. The minimization of objective function using appropriate numerical algorithm leading to identified model parameters of proposed constitutive model

Essentially, objective function can be defined as gap between measured and computed response values (displacement, stress, deformation, reaction force and etc.) (Imamovic *et al.* 2015)

$$J(\mathbf{d}_p) = \sum_{j \in J} w \left( \mathbf{u}_j^{com}(\mathbf{d}_p) - \mathbf{u}_j^{exp} \right)^2 \quad (20)$$

where  $\mathbf{d}_p$  are the model parameters we seek to identify, while  $\mathbf{u}_j^{com}$  and  $\mathbf{u}_j^{exp}$  are computed and experimentally (or numerically) measured values of displacement/strains/stresses, respectively and  $w$  is the weighting factor for different terms of objective function. The corresponding values for  $w$  have to be chosen in order to obtain similar norm of each summation term.

Minimization of objective function can formally be written as minimization under constraint

$$\min_{G(\sigma; \delta w)=0} J(\mathbf{d}_p) = \sum_{j \in J} w \left( \mathbf{u}_j^{com}(\mathbf{d}_p) - \mathbf{u}_j^{exp} \right)^2 \quad (21)$$

where the weak form of the equilibrium equations is the corresponding constraint.

The initial constrained minimization of objective function can be switched into unconstrained minimization by using Lagrange multiplier method (e.g., Ibrahimbegovic *et al.* 2004)

$$\max_{\forall \lambda} \min_{G(\sigma; \mathbf{d}_p)=0} L(\sigma, \mathbf{d}_p, \lambda) = J(\mathbf{d}_p) + G(\sigma, \mathbf{d}_p, \lambda) \quad (22)$$

where  $\lambda$  are Lagrange multipliers inserted into the weak form of equilibrium equations instead of the virtual displacement.

Since this type of minimization of objective function is very complex for large number of unknowns, this paper deals with splitting of the unconstrained minimization process of objective function into three completely independent stages owing to specific model structure. All the numerical computations are performed by using MATLAB and FEAP, which are linked during the whole computation process.

Table 1 Adopted material parameters for Timoshenko beams

General material parameters	Adopted Value
Young's modulus $E$	40000 MPa
Poisson's ration $\nu$	0.20
Axial yield stress in tension $\bar{\sigma}_x$	4.5 MPa
Axial yield stress in tension $\bar{\sigma}_y$	1.0 MPa
Axial yield stress in tension $\bar{\sigma}_z$	1.0 MPa
Material parameters for weakened elements <sup>a</sup>	Adopted value
Axial ultimate stress in tension $\bar{\sigma}_x$	4.5 MPa
Shear ultimate stress in tension $\bar{\sigma}_y$	1.0 MPa
Shear ultimate stress in tension $\bar{\sigma}_z$	1.0 MPa
Axial fracture energy in tension $G_{ft,x}$	0.06 N/mm
Shear fracture energy in tension $G_{ft,y}$	0.015 N/mm
Shear fracture energy in tension $G_{ft,z}$	0.015 N/mm

<sup>a</sup> Ultimate stresses and fracture energies for non-weakened elements are set to high values implying the softening phase cannot be reached

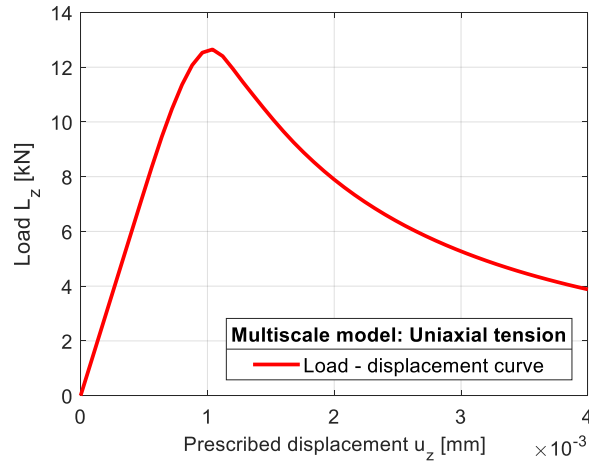


Fig. 7 Multiscale model results in terms of load-displacement curve for the compression test

In general, the complexity of identification procedure is influenced to a large extent by the choice of numerical or experimental setup. In the following, experimental setups numerically simulated in many examples are explained with the most important theoretical and practical settings.

#### 4.1 Tension test

In the context of the parameter identification, the simplest test to execute is simple tension test. However, this kind of test cannot be carried out experimentally, contrarily to steel. Hence, we carried out this only with respect to the numerical modeling. Multiscale model is utilized for that purpose whereas a 8-node hexahedron is chosen as a macro element and a total of 1838 Timoshenko beams are adopted as a micro-scale elements. In this way, the geometry of cube shaped specimen with sides equal to 50 mm is formed.

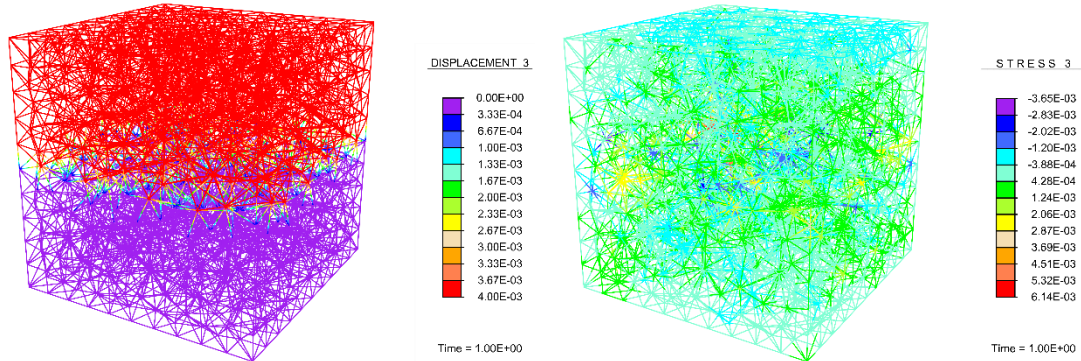


Fig. 8 Displacement and stress field at micro-scale at the end of numerical simulation

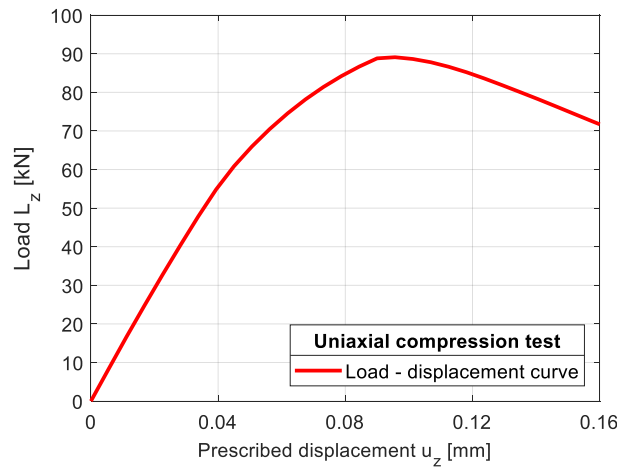


Fig. 9 Experimental load-displacement curve from compression test

In order to avoid localized failure in all micro-scale elements at the same time as well as numerical round-off errors, some elements in the middle of domain are weakened. The following table shows the general parameters of the material, as well as those corresponding to the weakened elements.

Global stress-strain diagram on multiscale can be divided into two parts which is in agreement with macro-scale response in tension: the first one which corresponds to the elastic response and the second one describing the softening regime.

The corresponding graphical representation of displacement and stresses at micro-scale is shown below.

Following the same pattern we can perform calibration of model parameters: first, from elastic part the bulk modulus  $K$  and the shear modulus  $G$  are determined, followed by elasticity limit stress  $\sigma_y$  and fracture energy in tension  $G_{f,t}$  estimated from softening part.

#### 4.2 Compression test

Compression test is surely the most performed experimental setup to obtain ultimate compressive

strength of concrete sample. Unlike the tension test, much simpler imposed load causes fairly different stress state leading to significantly different crack pattern and failure mechanism as well. Having in mind these statements, it is possible to identify parameters from each stage of deformation process including linear elastic, nonlinear inelastic and softening branch.

For the purpose of the parameter identification of previously mentioned Drucker-Prager plasticity model by using compression test as experimental setup, the same cube shaped geometry is considered. The experimental load-displacement curve used for the identification procedure is shown below.

## 5. Results of numerical simulation

Several numerical simulations for various kinds of experimental setups are performed to illustrate performance of the proposed methodology for identifying the corresponding material parameters.

### 5.1 Elastic phase

Following these tests (tension test, compression test, three-point bending test), elastic parameters tend to be the same, because concrete is statistically isotropic material (Ibrahimbegovic *et al.* 2020). Therefore, we adopt to identify tensile elastic parameters. For such identification procedure one can choose between two alternatives in terms of experimental setup: uniaxial tension test and three-point bending test. Practically, three-point bending test is not very convenient for experimental identification of elastic parameters due to the complexity of creating such setup for this kind of identification. Therefore, identification of tensile elastic parameters is preferentially carried out by including the numerical results of simple tension test obtained by multiscale model. However, three-point bending test can be very successfully simulated and predicted in the spirit of the multiscale approach as it shown in the work (Ibrahimbegovic *et al.* 2021).

In that context, objective function for identification elastic parameters  $G$  and  $K$  is given in the following form

$$J(G, K) = \left( L_{ref}(u) - L_{com}(u) \right)^2 w_1 + \left( \Delta l_{ref}(u) - \Delta l_{com}(u) \right)^2 w_2; \quad (23)$$

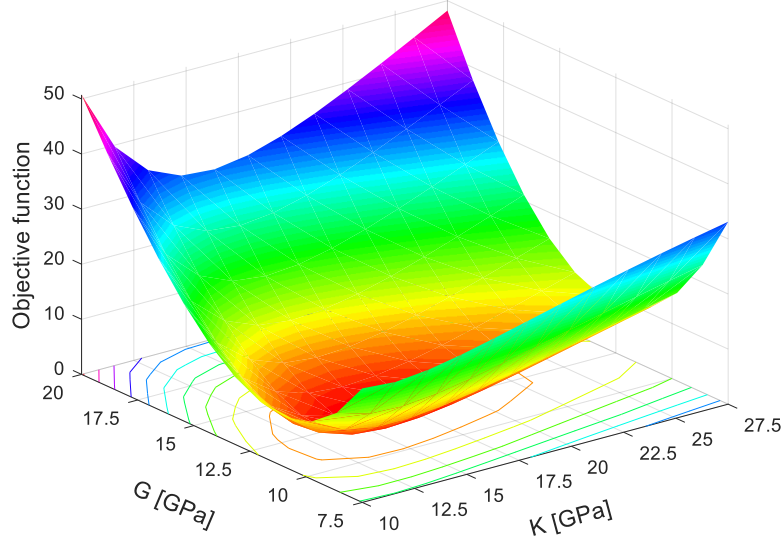
$$u = 0.0001 \text{ mm}$$

where  $L_{ref}(u)$  and  $L_{com}(u)$  are corresponding loads related to the target displacement  $u$  obtained in simple tension test on multiscale and macro-scale model, respectively. Similarly, the quantities  $\Delta l_{ref}(u)$  and  $\Delta l_{com}(u)$  are corresponding lateral elongations from multi-scale and macro-scale model, respectively.

Graphical representation of objective function  $J(G, K)$  is shown in Fig. 10. Objective function remains convex over the complete considered  $(K, G)$  domain, thus making optimization procedure rather computationally effective. The identified pair of elastic parameters is:  $(G^{opt}, K^{opt} = 12.56, 15.94)$  [GPa].

### 5.2 Hardening phase

Once we have successfully identified elastic parameters, we can carry on with estimation of the parameters of Drucker-Prager yield surface defined by the expression (2)

Fig. 10 Objective function  $J(G,K)$ 

$$\phi_y(\boldsymbol{\sigma}, q) := \|\text{dev}[\boldsymbol{\sigma}]\| + \frac{1}{3} \tan(\varphi) \text{tr}[\boldsymbol{\sigma}] - \sqrt{\frac{2}{3}} (\sigma_y - q)$$

where  $q$  is stress-like internal variable

$$q = -(\sigma_\infty - \sigma_y)[1 - \exp(-\beta\zeta)] - K_{h,lin} \cdot \zeta \quad (24)$$

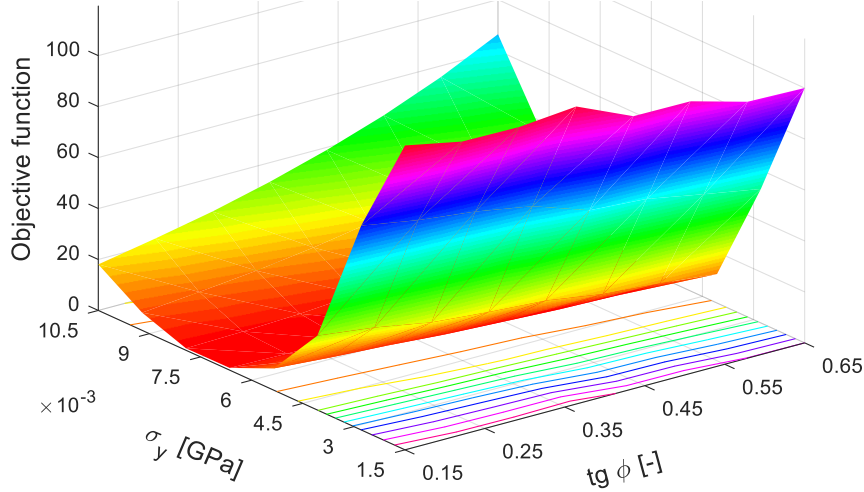
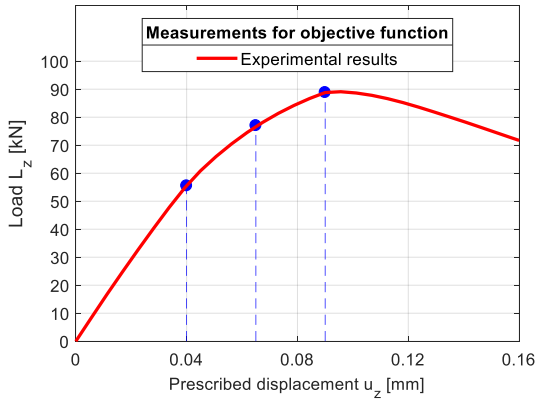
In the upper equation,  $\beta$  is the hardening parameter that governs the rate with which saturation is achieved,  $\sigma_\infty$  is the limit stress until the stress increase and  $K_{h,lin}$  is the hardening modulus. Taking the advantage of the proposed model, linear hardening can be simply obtained by assuming  $K_{h,lin} = 0$  while nonlinear hardening can be obtained by taking  $\beta = 0$ .

Identification procedure of hardening parameters is divided in the two separate and independent steps owing to the specific structure of the proposed macro-scale model. Indeed, the yield stress  $\sigma_y$  and internal friction parameter  $\tan(\varphi)$  are sufficient to define Drucker-Prager yield point in a unique way making it as a main point of consideration in the first step of hardening parameter identification. Objective function for the identification of the yield stress  $\sigma_y$  and internal friction parameter  $\tan(\varphi)$  is given in the following form

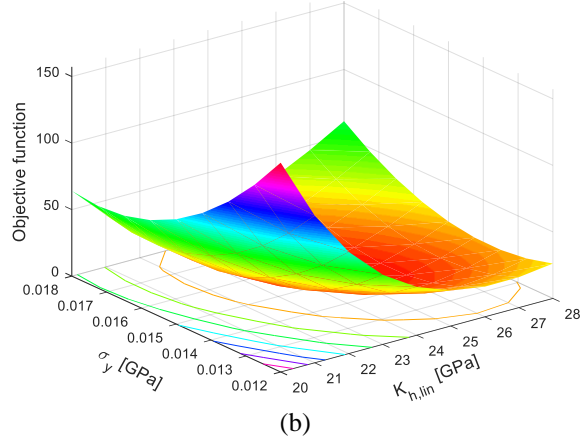
$$J(\sigma_y, tg\varphi) = (L_{ref,c}(u_y) - L_{com,c}(u_y))^2 w_1 + (V_{ref,c}(u_y) - V_{com,c}(u_y))^2 w_2 \quad (25)$$

taking into account load  $L$  and volumetric strains  $V$  from experimental uniaxial compression test and proposed macro-scale model for the target yield displacement  $u_y$ . Objective function  $J(\sigma_y, tg\varphi)$  for the hardening constitutive parameters using this approach is illustrated in Fig. 11.

The identified pair is  $\sigma_y^{opt} = 6.81$  MPa,  $tg\varphi^{opt} = 0.321$ . Concerning the second step, identification of linear hardening parameters is performed. In order to better approximate hardening behavior, notional yield stress is moved to the level when the residual plastic deformation is 0.2%. In this case, objective function is defined in the form

Fig. 11 Objective function  $J(\sigma_y, tg\phi)$ 

(a)



(b)

Fig. 12 (a) Measurements for objective function  $J(\sigma_y, K_{h,lin})$ , (b) objective function  $J(\sigma_y, K_{h,lin})$ 

$$J(\sigma_y, K_{h,lin}) = \sum_{i=1}^3 (L_{ref}(u_i) - L_{com}(u_i))^2 w_1 + \sum_{i=1}^3 (\Delta l_{ref}(u_i) - \Delta l_{com}(u_i))^2 w_2 \quad (26)$$

with a total of 3 measurements of load  $L$  and lateral elongation  $\Delta l$  on experimental setup and macro-scale model, respectively. Graphical representation of objective function  $J(\sigma_y, K_{h,lin})$  is shown in Fig. 12(b). Objective function remains convex over the complete considered  $(\sigma_y, K_{h,lin})$  domain, thus making optimization procedure rather straightforward. The identified pair of hardening parameters is:  $\sigma_y^{opt} = 15.27$  MPa,  $K_{h,lin}^{opt} = 24.52$  GPa.

In the Fig. 13, comparison between experimental results and macro-scale model is presented.

Obviously, linear hardening parameters are not sufficient for appropriate representation of real hardening behavior of concrete. Therefore, we should turn to another approach that better approximates the post-elastic phase of concrete deformation. This implies saturation (nonlinear)

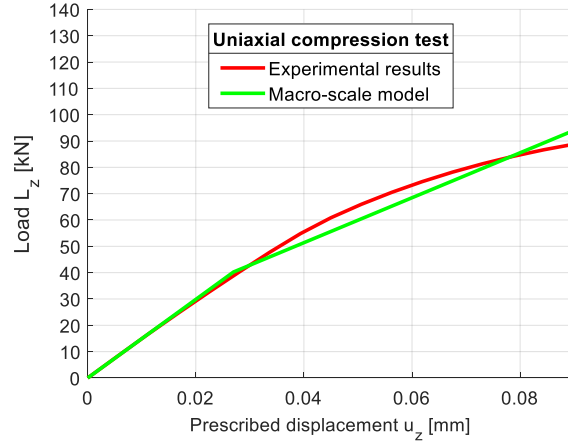


Fig. 13 Comparison between experimental and macro-scale model results for linear hardening

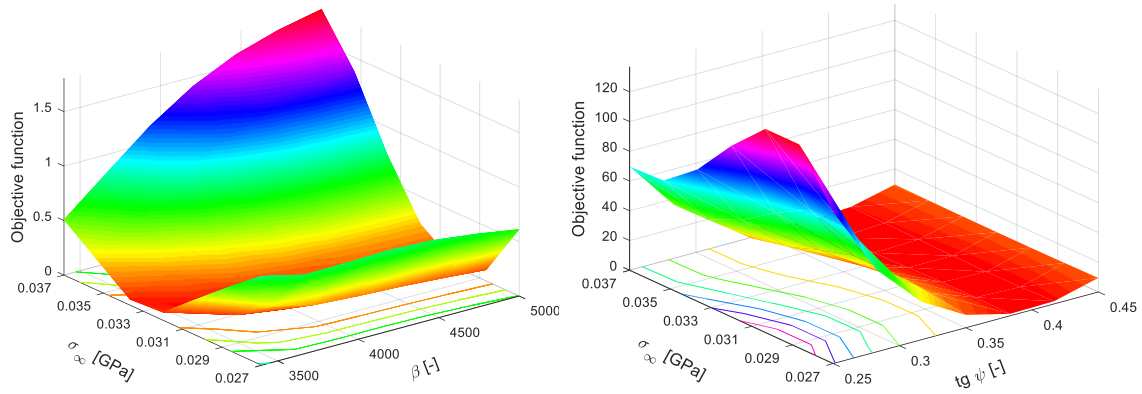


Fig. 14 Objective function  $J(\beta, tg\psi, \sigma_\infty)$

hardening, taking into account hardening parameter  $\beta$ , dilatancy parameter  $\tan(\psi)$  and  $\sigma_\infty$  as the ultimate stress. Objective function is constructed in the same manner as for linear hardening in the form, only now including three parameters

$$J(\beta, tg\psi, \sigma_\infty) = \sum_{i=1}^3 (L_{ref}(u_i) - L_{com}(u_i))^2 w_1 + \sum_{i=1}^3 (\Delta l_{ref}(u_i) - \Delta l_{com}(u_i))^2 w_2 \quad (27)$$

The graphical representation of objective function is presented in Fig. 14.

Comparison between experimental results and macro-scale model for saturation hardening is presented in Fig. 15.

Indeed, saturation hardening much more appropriate represents the microstructural response upon initiating and starting propagation concrete cracks comparing to linear hardening.

### 5.3 Softening phase

Firstly, identification of compression softening parameters is performed. According to the

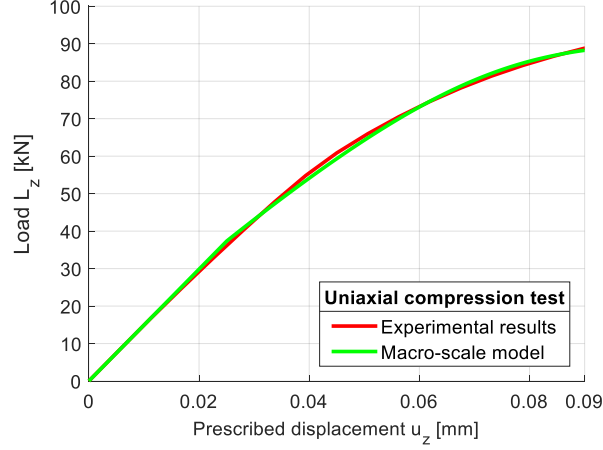
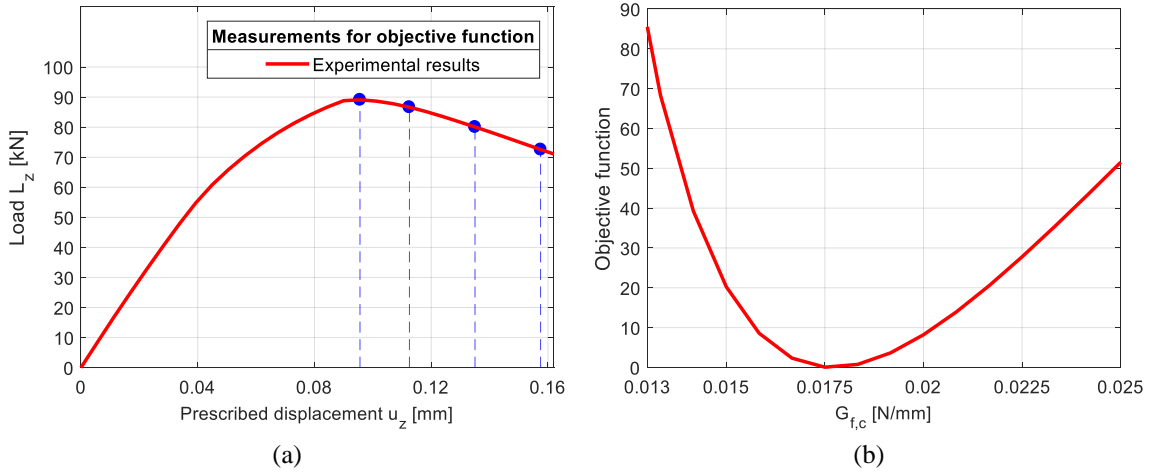


Fig. 15 Comparison between experimental and macro-scale model results for linear hardening

Fig. 16 (a) Measurements for objective function  $J(G_{f,c})$ , (b) objective function  $J(G_{f,c})$ 

specific model structure, identification of  $\sigma_\infty$  is already performed in previous stage making the fracture energy in compression  $G_{f,c}$  as the only parameter that should be identified. Therefore, it is sufficient to take into account just force measurement defining objective function in the following form

$$J(G_{f,c}) = \sum_{i=1}^4 (L_{ref,c}(u_i) - L_{com,c}(u_i))w_1 \quad (28)$$

The graphical representation of measurements for objective function is depicted in Fig.16a, while objective function  $J(G_{f,c})$  is shown in Fig. 16(b).

Comparison between experimental results and macro-scale model results for all different stages is presented in Fig. 17.

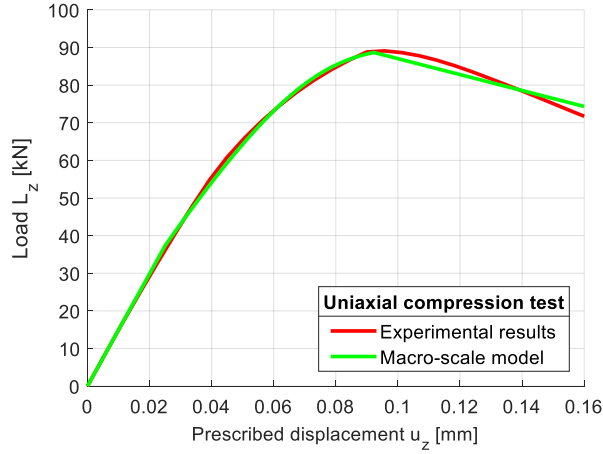


Fig. 17 Complete response comparison between experimental and macro-scale model results in compression

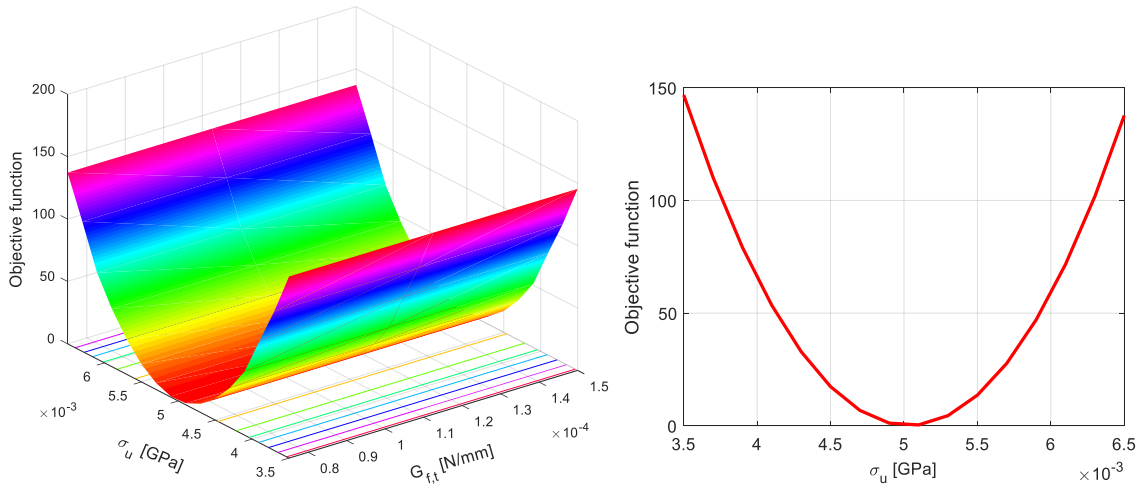


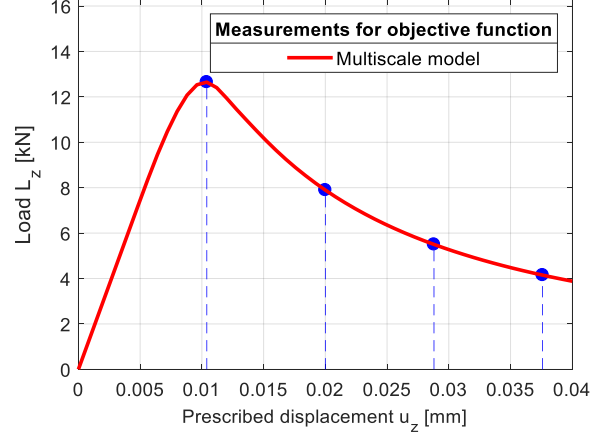
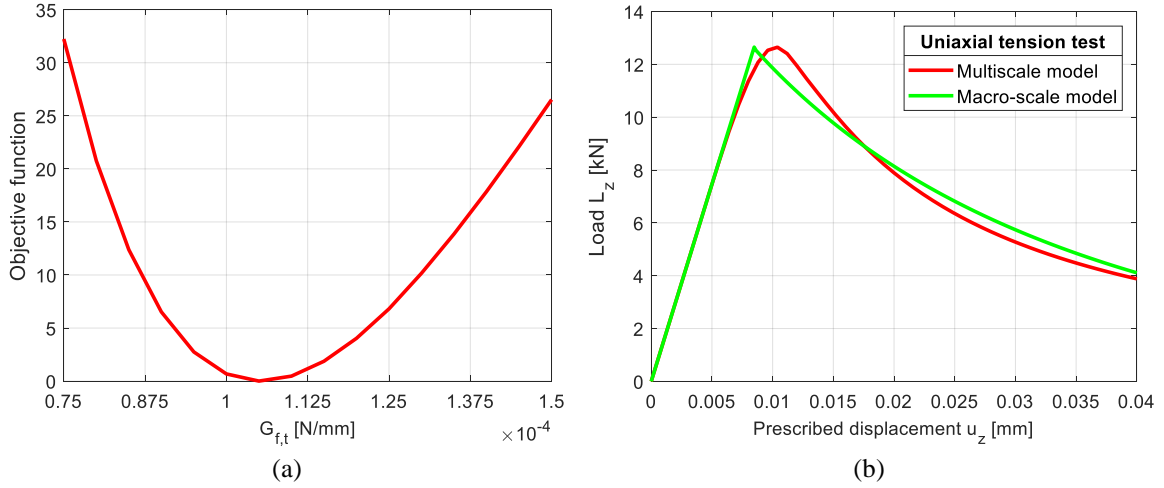
Fig. 18 Objective function  $J(\sigma_u)$

The identified value of fracture energy in compression is  $G_{f,c}^{opt} = 0.0175$  N/mm. Identification of tensile softening parameters involves the identification of ultimate stress which triggers softening in tension  $\sigma_u$  and fracture energy in tension  $G_{f,t}$ . Since, the value  $\sigma_u$  is independent from  $G_{f,t}$ , the corresponding objective function should be defined in the form:

$$J(\sigma_u) = (L_{com,max} \cdot \max_{ref,max}^2 w_1) \quad (29)$$

where  $L_{ref,max}$  and  $L_{com,max}$  are maximum loads (reactions) from the load-displacement diagram obtained in simple tension test on multiscale and macro-scale model, respectively.

The identified value of ultimate stress which triggers softening is  $\sigma_u = 5.04$  MPa. Having in mind the identified value of  $\sigma_u$ , we can identify the fracture energy in tension  $G_{f,t}$ . Similarly to the softening in the compression, a total of 4 load measurements are adopted for defining objective function.

Fig. 19 Measurements for objective function  $J(G_{f,t})$ Fig. 20 (a) objective function  $J(G_{f,t})$ , (b) comparison between multiscale and macro-scale model

Objective function can be written in the form

$$J(G_{f,t}) = \sum_{i=1}^4 (L_{ref,t}(u_i) - L_{com,t}(u_i))w_1 \quad (30)$$

where the subscript  $t$  denotes measurements on the tension test for multiscale and macro-scale model, respectively. Objective function  $J(G_{f,t})$  is shown in Fig. 20(a), and comparison between multiscale and macro-scale model in simple tension test is depicted in Fig. 20(b).

Objective function is convex and rather simple for optimization by adopted Nelder-Mead algorithm. The identified value of fracture energy in tension is  $G_{f,t} = 1.041 \cdot 10^{-4}$  N/mm.

As in the previous case for compression test, the results of the macro-scale model simulation carried out with optimized parameters fits very well with multiscale results for simple tension test as well.

### 5.4 Final remarks

The results provide very satisfying performance for all numerically simulated experimental setups. In addition to the diagrams, the efficiency of the Nelder-Mead optimization algorithm for the objective functions is presented. It can be concluded that proposed algorithm is rather computationally effective, since time of computation for all objective functions is in even greater extent optimized and reduced to reasonable degree. The related data are presented in the Table 2 below.

Table 2 The efficiency of the Nelder-Mead optimization algorithm

Objective function	Number of	
	Iterations	Evaluations
$J(G, K)$	38	72
$J(\sigma_y, tg\varphi)$	21	50
$J(\sigma_y, K_{h,lin})$	30	58
$J(\beta, tg\psi, \sigma_{sc})$	30	63
$J(\sigma_u)$	3	11
$J(G_{f,t})$	3	11
$J(G_{f,c})$	3	11

## 6. Conclusions

In this work, we evaluated the concrete parameter identification procedure by using real experimental measurements and numerical simulation results on multiscale model. The macro scale model is capable of describing elastic response, hardening with the Drucker-Prager plasticity model and full set of 3D failure mechanisms in softening. The numerical simulation of micro-scale model is one developed in the work (Ibrahimbegovic *et al.* 2021.). Identification procedure is based on Nelder-Mead optimization algorithm that proved very robust making the computation very effective in terms of computational time. The main ingredient that guarantees robustness is appropriate choice of cost function.

The identification procedure for elastic parameters is the most robust. Any of real experiments or numerical simulations is suitable to obtain the elastic parameters mainly either simple tension test carried out numerically, compression test or three point bending test carried out experimentally with result with equivalent values of elastic parameters. The reason is that concrete can be considered as statistically isotropic material, as already confirmed in the work (Ibrahimbegovic *et al.* 2020).

Identification of tensile softening parameters cannot be carried out experimentally. Mainly we cannot put concrete specimen in the simple tension-testing machine contrary to steel. However, the proposed multiscale modeling can be used to obtain very effectively the tensile yield stress and fracture energy in tension with the very robust computation using multiscale model. The simplicity of this procedure is in contrast against the complexity of three-point bending test on specially prepared concrete specimen with notches needed to obtain experimental results that in general used to determine the same tensile failure parameters.

The final conclusion concerns the identification of parameters for hardening in compression. We

show that different levels of more comprehensive measurements would result in more robust identification procedure than the one based upon force - displacement diagram (usual measurements in compression test). One can obtain linear hardening parameters but also show linear hardening parameters are not suitable for describing hardening behavior of concrete. We need something like the saturation hardening for more appropriate representing the experimental load-displacement curve. For identifying saturation hardening parameters, one should either add additional measurements for lateral displacements or use numerical simulation of dissipated energy in order to provide cost functions that are capable of making the identification procedure more robust.

## Acknowledgments

This work was supported by funding from ANR (project SELF-TUM), MEAE (project CESP) and IUF (project MS1479). Samir Suljevic also acknowledges the French Embassy in Bosnia and Herzegovina scholarship for doctoral studies in France. All this support is gratefully acknowledged.

## References

- Brancherie, D. and Ibrahimbegovic, A. (2008), "Novel anisotropic continuum-discrete damage model capable of representing localized failure: Part I: Theoretic formulation and numerical implementation", *Eng. Comput.*, **26**(1/2), 100-127. <https://doi.org/10.1108/02644400910924825>.
- Brancherie, D., Villon, P. and Ibrahimbegovic, A. (2008), "On a consistent field transfer in non linear inelastic analysis and ultimate load computation", *Comput. Mech.*, **42**(2), 213-226. <https://doi.org/10.1007/s00466-007-0199-1>.
- Chen, B. and Liu, J. (2004), "Experimental study on AE characteristics of three-point bending concrete beams", *Cement Concrete Res.*, **34**, 391-397. <https://doi.org/10.1016/j.cemconres.2003.08.021>.
- Claire, D., Hild, F. and Roux, S. (2004), "A finite element formulation to identify damage fields: The equilibrium gap method", *Int. J. Numer. Meth. Eng.*, **61**, 189-208. <https://doi.org/10.1002/nme.1057>.
- Furukawa, R. and Yagawa, G. (1997), "Inelastic constitutive parameter identification using an evolutionary algorithm with continuous individuals", *Int. J. Numer. Meth. Eng.*, **40**, 1071-1090. [https://doi.org/10.1002/\(SICI\)1097-0207\(19970330\)40:6<1071::AID-NME99>3.0.CO;2-8](https://doi.org/10.1002/(SICI)1097-0207(19970330)40:6<1071::AID-NME99>3.0.CO;2-8).
- Goldberg, D. (1989), *Genetic Algorithms in Search, Optimization and Machine Learning*, Addison-Wesley, Glen View, IL.
- Hadzalic, E., Ibrahimbegovic, A. and Dolarevic, S. (2019), "Theoretical formulation and seamless discrete approximation for localized failure of saturated poro-plastic structure interacting with reservoir", *Comput. Struct.*, **214**, 73-93. <https://doi.org/10.1016/j.compstruc.2019.01.003>.
- Hautefeuille, M., Colliat, J.B., Ibrahimbegovic, A., Matthies, H.G. and Villon, P. (2012), "Multiscale approach to modeling inelastic behavior with softening", *Comput. Struct.*, **94-95**, 83-95.
- Holland, J.H. (1975), *Adaptation in Natural and Artificial Systems*, MIT Press, Cambridge, MA.
- Hrstka, O. and Kucerova, A. (2004), "Improvements of real coded genetic algorithms based on differential operators preventing the premature convergence", *Adv. Eng. Softw.*, **35**(3/4), 237-246. [https://doi.org/10.1016/S0965-9978\(03\)00113-3](https://doi.org/10.1016/S0965-9978(03)00113-3).
- Hrstka, O., Kucerova, A., Leps, M. and Zeman, J. (2003), "A competitive comparison of different types of evolutionary algorithms", *Comput. Struct.*, **81**(18/19), 1979-1990. [https://doi.org/10.1016/S0045-7949\(03\)00217-7](https://doi.org/10.1016/S0045-7949(03)00217-7).
- Iacono, C., Sluys, L.J. and van Mier, J.G.M. (2006), "Estimation of model parameters in nonlocal damage theories by inverse analysis techniques", *Comput. Meth. Appl. Mech. Eng.*, **195**(52), 7211-7222. <https://doi.org/10.1016/j.cma.2004.12.033>.

- Ibrahimbegovic, A. (2009), *Nonlinear Solid Mechanics: Theoretical Formulations and Finite Element Solution Methods*, Springer, Dordrecht, Germany.
- Ibrahimbegovic, A., Knopf-Lenoir, C., Kucerova, A. and Villon, P. (2004), "Optimal design and optimal control of elastic structures undergoing finite rotations", *Int. J. Numer. Meth. Eng.*, **61**(14), 2428-2460.
- Ibrahimbegovic, A., Matthies, H.G. and Karavelic, E. (2020), "Reduced model of macro-scale stochastic plasticity identification by Bayesian inference: Application to quasi-brittle failure of concrete", *Comput. Meth. Appl. Mech. Eng.*, **372**, 113428. <https://doi.org/10.1016/j.cma.2020.113428>.
- Ibrahimbegovic, A., Rukavina, I. and Suljevic, S. (2021), "Multiscale model with embedded discontinuity discrete approximation capable of representing full set of 3D failure modes for heterogeneous materials with no scale separation", *Int. J. Multisc. Comput. Eng.*, **20**, 1-32. <https://doi.org/10.1615/IntJMCompEng.2021038378>.
- Imamovic, I., Ibrahimbegovic, A., Knopf-Lenoir, C. and Mesic, E. (2015), "Plasticity-damage model parameters identification for structural connections", *Couple. Syst. Mech.*, **4**(4), 337-364. <http://doi.org/10.12989/csm.2015.4.4.337>.
- Karakasis, M.K. and Giannakoglou, K.C. (2004), "On the use of surrogate evaluation models in multi-objective evolutionary algorithms", *ECCOMAS, 2004, 4<sup>th</sup> European Congress on Computational Methods in Applied Sciences and Engineering*, Jyvaskyla.
- Karavelic, E., Ibrahimbegovic, A. and Dolarevic S. (2019), "Multi-surface plasticity model for concrete with 3D hardening/softening failure modes for tension, compression and shear", *Comput. Struct.*, **221**, 74-90. <https://doi.org/10.1016/j.compstruc.2019.05.009>.
- Kozar, I., Toric Malic, N. and Rukavina, T. (2018), "Inverse model for pullout determination of steel fibers", *Couple. Syst. Mech.*, **7**(2), 197-209. <http://doi.org/10.12989/csm.2018.7.2.197>.
- Kucerova, A., Brancherie, D. and Ibrahimbegovic, A. (2006), "Material parameter identification for damage models with cracks", *Proceedings of the 8th International Conference on Computational Structures Technology*, Civil-Comp Press Ltd, Stirling.
- Kucerova, A., Brancherie, D., Ibrahimbegovic, A., Zeman, J. and Bittnar, Z. (2009), "Novel anisotropic continuum-discrete damage model capable of representing localized failure of massive structures- Part II: Identification from tests under heterogeneous stress field", *Eng. Comput.*, **26**, 128-144. <https://doi.org/10.1108/02644400910924834>
- Kucerova, A., Leps, M. and Skocek, J. (2005), "Large black-box functions optimization using radial basis function networks", *Proceedings of 8th International Conference on the Application of Artificial Intelligence to Civil, Structural and Environmental Engineering*, Ed. Topping, B.H.V., Civil-Comp Press Ltd, Stirling.
- Kucerova, A., Leps, M. and Zeman, J. (2007), "Back analysis of microplane model parameters using soft computing methods", *Comput. Assist. Mech. Eng. Sci.*, **14**(2), 219-242.
- Lagarias, J.C., Reeds, J.A. and Wright, M.H. (1998), "Convergence properties of the Nelder-Mead simplex method in low dimensions", *SIAM J. Optim.*, **9**(1), 112-147. <https://doi.org/10.1137/S1052623496303470>.
- Leps, M. (2005), *Single and Multi-Objective Optimization in Civil Engineering, Evolutionary Algorithms and Intelligent Tools in Engineering Optimization*, WIT Press, Southampton.
- Mahnken, R. (2004), "Identification of material parameters for constitutive equations", *Encyclopedia of Computational Mechanics, Part 2: Solids and Structures*, Chapter 19.
- Mahnken, R. and Stein, E. (1996), "Parameter identification for viscoplastic models based on analytical derivatives of a least-squares functional and stability investigations", *Int. J. Plast.*, **12**(4), 451-479. [https://doi.org/10.1016/S0749-6419\(95\)00016-X](https://doi.org/10.1016/S0749-6419(95)00016-X).
- Maier, G., Bocciarelli, M., Bolzon, G. and Fedele, R. (2006), "Inverse analyses in fracture mechanics", *Int. J. Fract.*, **138**, 47-73. <https://doi.org/10.1007/s10704-006-7153-7>.
- Michalewicz, Z. (1999), *Genetic Algorithms+Data Structures=Evolution Programs*, 3rd Edition, Springer, New York, NY.
- Nakayama, H., Inoue, K. and Yoshimon, Y. (2004), "Approximate optimization using computational intelligence and its application to reinforcement of cable-stayed bridges", *ECCOMAS 2004, 4th European Congress on Computational Methods in Applied Sciences and Engineering*, Jyvaskyla, Finland.

- Novak, D. and Lehky, D. (2006), "ANN inverse analysis based on stochastic small-sample training set simulation", *Eng. Appl. Artif. Intel.*, **19**(7), 731-740. <https://doi.org/10.1016/j.engappai.2006.05.003>.
- Pichler, B., Lackner, R. and Mang, H.A. (2003), "Back analysis of model parameters in geotechnical engineering by means of soft computing", *Int. J. Numer. Meth. Eng.*, **57**(14), 1943-1978. <https://doi.org/10.1002/nme.740>.
- Pyrz, M. and Zairi, F. (2007), "Identification of viscoplastic parameters of phenomenological constitutive equations for polymers by deterministic and evolutionary approach", *Model. Simul. Mater. Sci. Eng.*, **15**, 85-103.
- Waszczyszyn, Z. and Ziemianski, L. (2006), "Neurocomputing in the analysis of selected inverse problems of mechanics of structures and materials", *Comput. Assist. Mech. Eng. Sci.*, **13**(1), 125-159.
- Wilson, E.L. and Ibrahimbegovic, A. (1991), "A modified method of incompatible modes", *Commun. Appl. Numer. Meth.*, **7**, 187-194. <https://doi.org/10.1002/cnm.1630070303>.
- Yagawa, G. and Okuda, H. (1996), "Neutral networks in computational mechanics", *Arch. Comput. Meth. Eng.*, **3**(4), 435-512. <https://doi.org/10.1007/BF02818935>.